AD-A064 844 IBM THOMAS J WATSON RESEARCH CENTER YORKTOWN HEIGHTS N Y F/G 20/2
OPTICAL BI-REFRINGENT TECHNIQUE IN DEFECT CHARACTERIZATION.(U)
NOV 78 P CHAUDHARI F49620-77-C-0060

UNCLASSIFIED AFOSR-TR-79-0041 NL

AD | OF |
A064 844

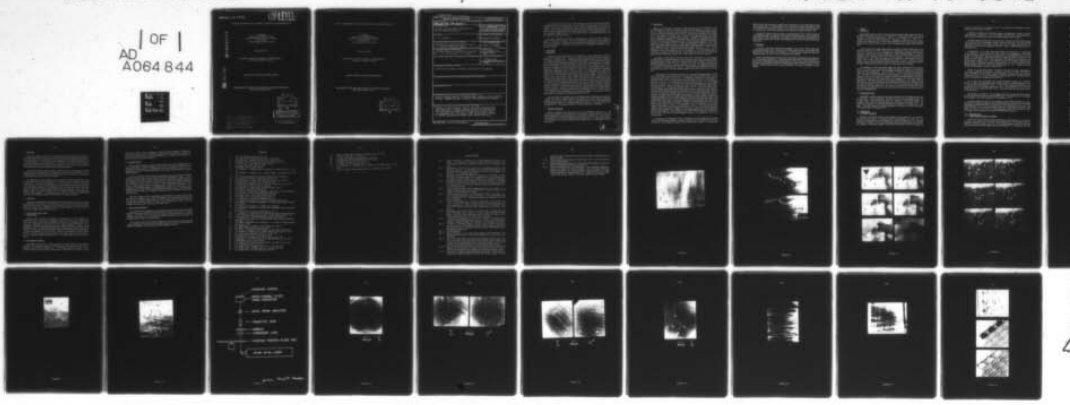

END
DATE
FILMED
4-79
DDC

AFOSR-TR- 79-0041

(13) LEVEL III

A058 311

OPTICAL BI-REFRINGENT TECHNIQUE IN DEFECT CHARACTERIZATION

P. Chaudhari
Thomas J. Watson Research Center
International Business Machines Corporation
P. O. Box 218
Yorktown Heights, New York 10598

30 November 1978

Final Report for Period 1977 March 01 - 1978 September 30
Contract No. F49620-77-C-0060

Approved for public release; distribution unlimited

SPONSORED BY THE AIR FORCE OFFICE OF SCIENTIFIC RESEARCH
AFSC, United States Air Force

OPTICAL BI-REFRINGENT TECHNIQUE IN DEFECT CHARACTERIZATION

P. Chaudhari
Thomas J. Watson Research Center
International Business Machines Corporation
P. O. Box 218
Yorktown Heights, New York 10598

30 November 1978

Final Report for Period 1977 March 01 - 1978 September 30
Contract No. F49620-77-C-0060

Approved for public release; distribution unlimited

SPONSORED BY THE AIR FORCE OFFICE OF SCIENTIFIC RESEARCH
AFSC, United States Air Force

UNCLASSIFIED

SECURITY CLASSIFICATION OF THIS PAGE (When Data Entered)

REPORT DOCUMENTATION PAGE	READ INSTRUCTIONS BEFORE COMPLETING FORM
1. REPORT NUMBER: AFOSR-TR-79-0041	2. GOVT ACCESSION NO. / 3. RECIPIENT'S CATALOG NUMBER
4. TITLE (and Subtitle): Optical Bi-Refringent Technique in Defect Characterization	5. TYPE OF REPORT & PERIOD COVERED: Final ~~Scientific~~ Report 1977 ~~Mar 1 1978 Sept 30~~ 1 May 77-30 Sep 78
	6. PERFORMING ORG. REPORT NUMBER
7. AUTHOR(s): P. Chaudhari	8. CONTRACT OR GRANT NUMBER(s): #F49620-77-C-0060
9. PERFORMING ORGANIZATION NAME AND ADDRESS: International Business Machines Corp. T. J. Watson Research Center P. O. Box 218, Yorktown Heights, NY 10598	10. PROGRAM ELEMENT, PROJECT, TASK AREA & WORK UNIT NUMBERS: Project No. 2306B2
11. CONTROLLING OFFICE NAME AND ADDRESS: Air Force Office of Scientific Research Bldg. 410, Bolling AFB, D.C. 20332	12. REPORT DATE: 1978 November 30
	13. NUMBER OF PAGES: 33
14. MONITORING AGENCY NAME & ADDRESS(if different from Controlling Office)	15. SECURITY CLASS. (of this report): Unclassified
	15a. DECLASSIFICATION/DOWNGRADING SCHEDULE

16. DISTRIBUTION STATEMENT (of this Report)

Approved for public release; distribution unlimited

17. DISTRIBUTION STATEMENT (of the abstract entered in Block 20, if different from Report)

18. SUPPLEMENTARY NOTES

19. KEY WORDS (Continue on reverse side if necessary and identify by block number)

Stress induced optical bi-refringence, defects, GaP, Garnets, Silicon, Ribbon Silicon, Devices, Non-Destructive Testing

20. ABSTRACT (Continue on reverse side if necessary and identify by block number)

Defects in GaP, Garnets, and Si have been examined and characterized by stress induced optical bi-refringence. This technique is explored in examining devices and it is suggested that its utility lies in the early stages of device fabrication rather than towards the end.

DD FORM 1 JAN 73 1473 EDITION OF 1 NOV 65 IS OBSOLETE

UNCLASSIFIED

SECURITY CLASSIFICATION OF THIS PAGE (When Data Entered)

349250

This contract called for a study of the usefulness of the stress induced birefringent technique to examine, non-destructively, defects in device related materials. In this one-year contract period, we have examined GaP, garnets, (useful for bubble technology) and silicon crystals. We have observed dislocations, grain boundaries and other defects in garnets. In silicon we have examined dislocations, growth induced strains and other inhomogeneities. We have attempted, without success, to examine actual devices, ion implantation strains, and laser-induced crystallization in silicon.

This report is divided into five parts. In the first two we describe our work on GaP and garnets. In the third, we present our work on dislocations in silicon and, in the fourth, we summarize our results on a variety of device related processes associated with silicon technology. In the final part we comment on the utility of the birefringent technique for non-destructive testing.

1. GaP Crystals

1.1 Introduction

Advances in crystal growth have led to fabrication of large crystals that are free, or almost free, of dislocation lines. Much of the impetus for this advance has been provided by the needs of electronic devices. Dislocations have deleterious effects in silicon transistors [1], magnetic bubble devices [2], and heterojunction lasers [3,4], and have led to specifications for crystals which include upper limits to the density of dislocation lines. The importance of dislocations in devices has made it necessary to have a simple, rapid, and non-destructive technique for determining the dislocation content of large crystals. There are, at present, two techniques that one might use. One is the optical birefringence technique discovered by Bond and Andrus [5], and the other is x-ray topography [6]. Both these methods are nondestructive and enable the Burgers vector and signs of dislocations to be found [6-9]. The advantage of birefringence is that it can be applied to crystals that are thick as well as large in lateral extent. Indeed, birefringence becomes easier to use as the thickness of the crystal increases. The reason for this is that the size of a birefringence image of a dislocation increases as the length of the optical path in the strain field of the dislocation is increased. The disadvantages of birefringence are that it can only be applied to materials that are transparent to visible, ultra-violet, or infrared radiation, and it is difficult to apply to substances where the elasto-optical coefficients [10], the refractive index, and the Burgers vectors, are small. A group of crystals for which birefringence images of individual dislocations are expected to be difficult to obtain are the alkali halides [11-14]. Kear and Pratt [15] studied the plastic deformation of LiF using birefringence and found that trains of dislocations were discernible but individual dislocations were not.

Here we describe the application of the birefringence method to dislocations in large GaP crystals. This work is a simple extension of that carried out on large crystals of gadolinium gallium garnet (or GGG) [16]. GaP is a convenient material to use to test the application of the birefringence technique to semiconducting crystals because it has large elasto-optical coefficients [17], a large refractive index (~3), and is transparent to visible light.

1.2 Specimen preparation

GaP was synthesized from the elements by a vertical Bridgman technique [18]. The polycrystalline product of this synthesis was converted into a large single crystal using the liquid encapsulation Czochralski method and a boric oxide encapsulant [19]. The crystal was oriented with the [111] direction parallel to the growth axis. A (111) slice approximately 1 cm in thickness was cut from it and polished (with 0.05μm Al_2O_3) for examination by optical microscopy.

1.3 Observations

Figure 1 is a micrograph of a portion of a GaP crystal that was one cm in thickness. The features labelled D are images of dislocations with lines almost parallel to the optic axis and the [111] direction in the crystal. The microscope was set so that the plane imaged in sharp focus lay 4 mm below the upper surface of the slice. The polarizer and analyzer were inclined at 45° to the borders of the figure. The [112] and [110] directions shown on the figure were determined by the Laue back reflection method. Comparison of the dislocation images with the predictions of Bullough [7] (modified to take account of a superimposed long range stress [20,21]) shows that all dislocations in Fig. 1 have a large edge component, and that the projection of this component in the (111) plane was approximately parallel to [110]. This result, taken together with the geometry of the complete dislocations expected in GaP crystals [22], suggests that there is only one conclusion to be drawn from Fig. 1. This is that the dislocations were in edge orientation and that their Burgers vectors were $\pm 1/2$ a [110]. Although the sign of the dislocations was not determined, it is worth remarking that the dislocations in the Figure had the same sign. The evidence for this is that, in all dislocation images, the pale portion of the images lay on the left and the dark portion on the right.

The number of dislocations per unit area of Fig. 1 was $\sim 5 \times 10^4$ per cm^2. It is clear that dislocations with an average separation of about one third of that in Fig. 1 could be examined by the birefringence method. This means that the method could be applied to crystals with a dislocation density of $\sim 5 \times 10^5$ per cm^2. A density of $\sim 10^5$ per cm^2 is about the lowest that can be conveniently studied by transmission electron microscopy. The highest density that can be examined by TEM exceeds 10^{11} per cm^2. Thus, birefringence combined with electron microscopy can be used to examine dislocation densities that range from zero to $> 10^{11}$ per cm^2.

A consequence of the high refractive index (n) of GaP, and other semiconductors, is that only a small fraction of the dislocations in crystals with parallel polished surfaces can be examined *end-on* like those in Fig. 1 [23]. If a dislocation is inclined at $r°$ to the normal to the crystal surface than $i°$, the tilt needed to bring the dislocation into the *end-on* position, is given by $\sin i / \sin r = n$. The maximum value of i is 90° and n for GaP is ~3. The maximum value for r is therefore 19.5°. This angle can be increased by immersing the crystal in a liquid with high refractivity. However, the gain is not large. Immersion of GaP into a liquid with a refractive index of 1.7 increases the maximum value of r to 35°. These facts make it important to determine whether dislocations in GaP can be seen when their lines are not parallel to the path that the imaging light beam takes through the crystal. Observations made on garnets [24-26], and other less symmetric crystals [27], have shown that dislocations with lines inclined to the light beam are discernible if the specimen is suitably oriented with respect to polarizer and analyzer. However, similar observations have not been reported for dislocations in semiconducting crystals [21,28,29] unless they were heavily decorated with copper. The observations we have made on GaP have demonstrated that dislocations with lines steeply inclined to the optical path are discernible. Examples of dislocations inclined to the optical path are seen in Figs. 2a and 2b. The micrographs in Fig. 2 are images of the same area. However, the specimen was raised 0.1 mm between (a) and (b). This means that the plane imaged in sharp focus was 0.3 mm higher in (b) than in (a). It can be seen that this change in elevation was accompanied by a translation of the sharply imaged portion of each dislocation along the dislocation line. This translation varied a little from one dislocation to another but was ~0.2 mm. This means that the dislocations in Fig. 2 were inclined at ~56° to the specimen plane.

The contrast at the dislocations in Fig. 2 is believed to have arisen largely from the strain fields of the dislocations themselves. Evidence in support of this is provided by the fact that the contrast at the dislocations changed from one dislocation to another. The dislocations

labelled A to F were dark above and light below. Dislocation G, on the other hand, was light above and dark below. A contrast change of this type would be expected if the Burgers vector of G was different to the Burgers vectors of A to F. However, a contrast difference would not be expected if the contrast at the dislocations was dominated by precipitate particles [28].

Although it is apparent that the contrast at the dislocations in Fig. 2 was not dominated by precipitate particles, it is important to note that the dislocations in Fig. 2 were decorated by small particles. These particles may have modified the strain fields of the dislocations and altered their visibility a little [23,30]. Decorating particles were not detected on the dislocations in Fig. 1.

1.4 Discussion

It has been found that stress-induced birefringence can be used to follow dislocations through large crystals of GaP. Dislocations are visible whether their lines are parallel to the path taken by the light beam or are inclined to it. The observations suggest that dislocation densities as high as 5×10^5 per cm^2 can be examined by the method.

The fact that dislocations with lines parallel and inclined to the light beam are discernible has one noteworthy consequence. It means that Tanner and Fathers' [20] detailed theory of the contrast in birefringence images of dislocations in crystals can be used to determine the geometry of dislocations in large crystals (of materials like GaP) in much the same way as the theory of electron images is used to analyze dislocations in electron micrographs of small samples.

2. Garnets

2.1. Introduction

Many bubble domain devices are made by depositing magnetic garnet films onto wafers of gadolinium gallium garnet ($Gd_3 Ga_5 O_{12}$ or GGG) (31). A much smaller number are prepared on wafers of neodymium gallium garnet ($Nd_3 Ga_5 O_{12}$ or NdGG) (32). However, it is possible that the use of NdGG will increase. Advantages of NdGG are (a) that is has a relatively low melting point (33) is easier to grow than GGG, and (b) that its lattice parameter matches those of garnets which are able to provide minimally small magnetic bubble domains (32).

A crucial factor in the performance of devices prepared on GGG or NdGG wafers is the dislocation content of the films. Dislocations are important because they impede bubble motion (2). Etch pits (34), X-ray topographs (35), and birefringence images (36) of dislocations have revealed that the majority of dislocations in films are simply extensions of those that terminated on the substrate surface before film growth began. Thus, the elimination of dislocations from garnet films must begin with the preparation of dislocation-free substrate wafers. This, in turn, requires that dislocation-free boules be grown. Advances in crystal growth have led to routine production of GGG crystals that are free or almost free of dislocation lines. Dislocation-free crystals of NdGG have been grown but not routinely.

The similarities of GGG and NdGG suggest that similar dislocations will be found in them. To test this we have examined dislocations in NdGG wafers using the etch pit method, and stress induced birefringence. The birefringence technique was discovered by Bond and Andrus (5) and first applied to a garnet ($Y_3 Ga_5 O_{12}$ or YGG) by Prescott and Basterfield (37). This early work was followed by many investigations of GGG using the birefringence method (9, 24-26). The results were consistent with Prescott and Basterfield's observations, and with other studies of GGG made using X-ray topography (38). The optical images of dislocations in GGG also revealed that stress-induced birefringence is more versatile than had been realized. The images demonstrated that dislocations did not need to be along the optical axis of the microscope in order (24-27) to be seen. They also showed that the method could be applied to very large crystals (39). The only other non-destructive technique that can be used to examine dislocations in crystals that are thick as well as large in lateral extent seems to be neutron topography (40).

2.2. Experimental Details

Large NdGG crystals were grown from iridium crucibles by the Czochralski technique and cut into wafers ~ 0.5 mm in thickness. The surfaces of the wafers were parallel to the (111) or (100) planes. Some wafers were etched in a mixture of concentrated sulphuric and phosphoric acid to form pits where dislocation lines terminated on the sample surface. All wafers were examined in a polarizing microscope with polarizer and analyser set at right angles. The wafers selected for detailed examination were much less perfect than average: they contained about 10^4 dislocations/cm^2.

2.3. Observations

2.3.1 Threading Dislocations

Examples of dislocations with lines that extended from one surface of a (111) wafer to the other are seen in Fig. 3. This figure contains six micrographs of the same area. The microscope was focussed on the lower surface in (a) and on the upper one in (f). Triangular etch pits are visible in (a) and (f), and birefringence images of the dislocations can be seen in the remainder. Dislocations labelled A and B cross one another on their way through the

crystal: A is above B in (a) and below (b) in F. This would have been difficult to deduce from the images of the etch pits along.

Dislocation C appears to go through the sample at an oblique angle. However, measurements show that it is inclined at ~ 12° to the normal to the wafer plane. The illusion that it is more obliquely inclined than this results from the high refractive index of NdGG.

Etch pits labelled D can be seen in (a), (b) and (f). However, these pits differ from the others present in that no birefringence image is associated with them. This, taken together with the fact that D in (a) lies almost vertically above D in (f), suggests that the dislocation responsible for D was in screw orientation (27,41-43). If this is so then the Burgers vector of D was along (111).

The images of E, F, G, H and I show that their lines were inclined at $\lesssim 7°$ to the normal to the wafer plane. As the plane of the wafer in Fig. 3 was perpendicular to the growth direction this result means that many dislocation lines were approximately but not precisely parallel to the growth axis. Similar results have been obtained for GGG by Glass (43). The images of E and I suggest that the edge components of their Burgers vectors (projected into the film plane) lay along <112>. If we assume this result, and, in addition, assume that the Burgers vectors of dislocations in garnets lie along the <111>, <110> or <100> directions, then the Burgers vectors of E and I were probably parallel to <111>. However, it is also possible that their Burgers vectors were along <110>.

Figure 4 is a series of micrographs of a portion of an etched (100) wafer. Micrograph (a) is the lower surface and (f) the upper. The edges of the pits is (a) and (f) lie along the <001> directions in the (100) plane. Dislocations labelled A and B move from left to right as one goes from (a) to (f). D, on the other hand, moves from right to left. The inclination of A and B to the normal to the sample plane was about 15°.

Pit C in Fig. 4(a) is associated with a single birefringence image in (b). However, between (b) and (c) the birefringence image changes from that of a single dislocation into that of a pair of dislocations labelled C' and C". C' and C" move further apart between (c) and (d) and give rise to a pair of clearly resolved pits in (f). The dissociation of C into C' and C" means that there was a dislocation node in Fig. 4. Dislocation nodes have been found in GGG but were rare (16).

The contrast at E in Figs. 4(c) and (d) suggests that the edge component of E (projected into the film plane) was parallel to the horizontal border of the figure. This in turn suggest that the Burger vector of B was parallel to (110), possibly, or (111).

A feature of Figs. 4(e) and (f) is the presence of three small pits labelled a, b and c. These pits are unlike those associated with threading dislocations and there is no discernible birefringence associated with them. Also they do not have counterparts in Fig. 4(a). (The feature labelled s in (a) is a scar on the sample surface and not the image of an etch pit). The origin of a, b and c in Fig. 4(f) has not been determined. However, observations on GGG (21) suggest that they may have been caused by small precipitate particles.

2.3.2 Dislocation loops

2.3.2.1 Loops around precipitates or inclusions

Fig. 5 shows a pair of dislocation loops that encircle an iridium inclusion in a (111) wafer. The plane of the loops is (111), and the loops themselves go out of contrast when the polarizer or analyser is parallel to their line. These features suggest (20,44,45) that the loops were prismatic and that their Burgers vectors were parallel to (111) Prismatic loops that

encircled iridium inclusions and had Burgers vectors along <111> have been observed in GGG (10).

A feature of the loops in Fig. 5 is the presence of precipitate particles, like P, along them. Precipitates have recently been observed at loops in GGG (44). However, the primatic loops in the early GGG crystals (24) did not have discernible precipitates associated with them.

Fig. 6 shows a pair of loops L_1 and L_2 around a small dark particle in an (001) wafer. The inclination of the loops to the wafer surface, and the fact that they lie on a plane which intersects (001) along (100), shows that they were approximately parallel to the (011) plane. Comparison of the loops in Fig. 6 with the (011) loops found in GGG (10) suggests that the loops in Fig. 6 were prismatic and that their Burgers vectors were parallel to (011).

The feature labelled I in Fig. 6 is an out of focus image of an iridium inclusion. The composition of the two dark dots inside L_1 and L_2 is not known.

Although the loops in Fig. 5 and 6 are amongst the largest found in NdGG, and are much larger than those commonly found in crystals, they are smaller than those observed in GGG (24,38). The largest loops in GGG were about ten times the diameter of those in Figs. 5 and 6.

2.3.2.2 Small loops on {110}

High magnification images of NdGG crystals have revealed many prismatic loops significantly smaller than those described in 3.2.1. The loops lay on {110} planes and did not have visible precipitates at their centers. However, it should be emphasized that it is possible that *precipitates were present but did not absorb or scatter sufficient light to be seen.*

Examples of the small loops are labelled A and B in Fig. 7. The loops in Fig. 7 lay on a {110} plane perpendicular to the film plane. Their images are the same as those expected from pairs of edge dislocations of opposite sign (41,42,46). The orientation of the edge dislocations were such that Burgers vectors of the dislocations were perpendicular to the line joining them.

Evidence that the pairs of dislocations in Fig. 7 were the opposite sides of loops, and not threading dislocations of opposite sign, is provided by the fact that the dislocations were clearly visible at only one setting of the microscope. If the microscope was either raised or lowered the dislocation contrast gradually disappeared. This is demostrated by the two parts of Fig. 7. The microscope was raised 6 μm between the recording of (a) and (b). The dislocations labelled A are sharply imaged in (a) but not in (b). Thosed labelled B are sharply imaged in the (b) but not in (a).

The diameters of the loops in Fig. 7 were 8.5 and 7.2 μm. The smallest loop we have seen was 3.1 μm in diameter. This seems to be the smallest loop that has been observed by stress-induced birefringence. It is of some interest to compare its diameter with the diameters of loops observed by other methods. Rabier et al. (47) have observed loops in yttrium iron garnet using transmission electron microscopy. The largest loop they found was about one sixth of the diameter of the smallest loop that we have seen. The smallest loops detected by X-ray topography (48,49) are much larger than the smallest loops that we have seen. The smallest loop that could be observed by the decoration method (50) is fixed by the resolution unit limit of the light microscope. It is thus about one tenth of the diameter of the smallest loop observed in NdGG.

2.3.3 Burgers vectors of Dislocations

The results in Sections 3.1 and 3.2 indicate that dislocations with Burgers vectors along <110> and <111> were present in NdGG. However, the results in these sections do not provide evidence for dislocations with Burgers vectors along <100>. The purpose of this section is to point out, that, although we do not have compelling evidence for Burgers vectors along <100>, we have made many observations that are consistent with the presence of dislocations with Burgers vectors along <100>. Fig. 8(a) shows a portion of the surface of an etched (100) wafer. Fig. 8(b) is a birefringence image of the dislocation in the interior of the sample. The images of the four dislocations near the center of Fig. 8 show that their lines were almost parallel to the optical axis, that they had large edge components, and that the projections of these components lay along the (100) direction in the (001) wafer plane. If we assume (9,10) that the dislocations in garnets have Burgers vectors along <111>, <110> or <100> then the Burgers vectors of the dislocations near the center of Fig. 8 lay along (100) or (101).

2.3.4 Absence of Helical Dislocations

Imperfect GGG crystals contained unusually large helical dislocations (26,35). Helical dislocations have not been found in NdGG crystals.

2.3.5 Low-angle Grain Boundaries

Imperfect NdGG crystals contained a number of very low-angle grain boundaries. The boundaries resembled those in GGG (34) in that their structure varied greatly along their length. Some parts of the boundaries consisted of regularly spaced parallel dislocations. Other parts were made up of rather irregularly arrange dislocation lines. The boundary in Fig. 9 consists of regularly arranged dislocations near A and rather irregularly arranged one elsewhere. The pairs of dislocations labelled a, b and c resemble the paired dislocations found in grain boundaries in germanium and silicon crystals by Oberly (51) and Okada (52).

A portion of a grain boundary in which the arrangement of dislocations is different from that usually assumed for low-angle boundaries, and different from the less regular arrangements studied by Oberly and Okada, is seen in Fig. 10. The boundary in this figure consists of two almost parallel columns, x and y, of dislocations which have large edge components and lines approximately parallel to the optic axis. The image contrast at the dislocations shows that they were all of the same size (20,24,46) and that their Burgers vector (41) projected into the wafer plane lay along (110). A feature of x and y is that the dislocations in y fall into the gaps between the dislocation in x. This holds even when there is a dislocation missing from x or y. Similar arrangements of edge dislocations have been observed in crystals of GGG (see Figs. 24(b) and 11 of Ref. 10). If we assume that the Burgers vectors of the dislocations in Fig. 10 were a (110) then the station across the boundary was $\sim 10^{-6}$ deg.

2.3.6 Two Features of Birefringence Images of Dislocations

Two features of birefringence images of dislocations are shown by Fig. 10. The first is that the size of the image of a dislocation depends upon the distance between the dislocation and its neighbors. For example, the image of the rather isolated dislocation labelled G is larger than the image of F which has a number of near neighbors. Also, the images of dislocations and D are larger than the image of B. The explanation for this phenomenon is that the birefringence image of a dislocation occupies the region where the dislocation's elastic strain field dominates over the strain fields of the other dislocations present. This feature of birefringence images has some practical importance. If the dislocation density in a crystal is low the images of individual dislocations are larger and low magnification images can be used to observe them. On the other hand, if the dislocation density is high the images are small and closely spaced dislocation can be resolved. The dislocation density at which individual

dislocations become difficult to observe by the birefringence method is not known. However, the observation of a loop ~ 3 μm in diameter suggests that it is about $10^7/cm^2$.

The second feature shown by Fig. 10 is that dislocations are easy to observe if the background contrast is gray but are rather difficult to detect if the background is black. This can be seen by comparing the image of dislocation A with the images of the dislocations in the lower portion of the figure. The visibility of A becomes comparable with that of the dislocations in the lower half of the figure if the exposure is increased by a factor of five or ten.

Black backgrounds to dislocations are obtained when the medium surrounding the dislocations is either unstressed or stressed in such a way as not to change the polarization of the incident light beam. Grey backgrounds (and dark and light lobes in the dislocation images) result from long layer stresses that do change the polarization of the incident light beam (10,15,23).

2.4. Conclusions

Imperfect NdGG crystals have been found to contain long straight dislocations, large straight dislocations, large prismatic loops, small prismatic loops, dislocation nodes, and grain boundaries of very low angle. The large prismatic loops encircled iridium inclusions, or unidentified precipitate particles, and often had precipitate particles found along them. The small loops did not have visible precipitates or inclusions associated with them. They are thought to be the smallest loops that have been observed by the birefringence method.

Some dislocations had Burgers vectors along <111>. Others had Burgers vectors along <110>. Dislocations with Burgers vectors along <100> may have been present but we do not have conclusive evidence for this.

Birefringence images of dislocations are larger when the dislocation density is low but small when their density is high. Thus, low magnification images can be used to examine the dislocations in large, almost perfect, crystals. High magnification images can be used to observe individual dislocations in crystals that may contain as many as ~ 10^7 dislocations per cm^2.

3. Dislocations in Silicon Crystals

3.1 Introduction

Dislocations in silicon have been imaged by numerous investigators (5, 46, 53, 54) using the piezobirefringence effect, but until now only lines viewed end-on or large groups of dislocations produced detectable contrast. In comparison, birefringence images of dislocations can be detected at any orientation in some other transparent crystals, such as gadolinium gallium garnet and barium titanate, because of their large strain optic constants. Several papers have discussed the visibility criteria for images in these materials.

We have observed, for the first time, birefringence images of dislocation lines in Si which are not viewed end-on and also comment on the criteria for the visibility of such dislocation lines. The observation of images were made on (111) wafers where most dislocations are not perpendicular to the wafer surface. Dislocation images were also observed in (100) and (110) wafers which were not viewed end-on, but these results are not reported here.

3.2 Experimental

The equipment required for this study consisted of a transmission microscope with a nicol prism analyzer, a 50 mw HeNe laser tuned to 1.15μm line, and a microchannel plate image converter,* set up as shown in Fig. 11.** The laser beam was sufficiently polarized that a polarizer was not required. Photographs were taken from the phosphor screen of the image converter. A wobbling ground glass disc was rotated below the condenser lens to remove unwanted interference fringes from the image. Another set of strong interference fringes produced within the image converter was eliminated through the simple expedient of randomly moving the device in the horizontal plane during the exposure. Before removal of the fringes, individual dislocations were very difficult to see.

The specimens used were undoped (111) silicon slices 2 to 3 mm thick which were polished on each side using the cupric ion chemical/mechanical technique. The dislocation density was fairly low (of the order 10^2 lines cm^{-2}).

3.3 Results

Figures 12 through 15 show images of various groups of mixed dislocations. Some of the specimens were given in light Sirtl etch (1 part 33% CrO_3:2HF: $2H_2O$) to develop etch pits at points of emergence of dislocation lines. These pits provided confirmation that the features observed were indeed individual dislocation lines. The contrast at the lines was greatest in each case when the line direction was oriented 45° to the direction of polarization. When the line directions coincided with the polarizer or analyzer, the contrast apparently vanished in each case. Each dislocation line image was light on one side and dark on the other. This image form is the result of the interaction of fairly uniform long range strain fields in the crystal with the dislocation strain field (23).

---

*The microchannel plate image converter was supplied by ITT, Electro-Optical Products Division, Fort Wayne, Indiana, 46803 USA.

**In place of the microchannel plate converter we have also been able to obtain similar dislocation images with a commercially available Hammamatsu TV camera and display system. This system projects images onto the screen and has the advantage of measuring light intensity spatially.

3.4 Discussion

The work of Tanner and Fathers (23) suggests that pure edge dislocations in the plane of observation should behave as those observed here, while pure screw dislocations should be 45° out of phase, that is, they should offer the maximum contrast when aligned with the analyzer or polarizer direction. In the present work, no examples of screw dislocation behavior were seen, although numerous curved segments were to be found. In a few places, lines seemed to terminate without the crystal, and the missing segments were not visible in any orientation. Also, many etch pits had no dislocation contrast associated with them.

The observed behavior suggests that the contrast caused by edge components is much stronger than that arising from screw components, and that the edge components rule in the visibility behavior. The fact that the present dislocations do not always lie in the plane of observation may also have an effect on the results.

The achievement of these images is due in large part to the laser light source. The monochromaticity and excellent polarization of the beam enhance the resolution and contrast of the images. These same characteristics of the laser also lead to a host of distracting interference effects. Most of the unwanted effects arising within the specimen can be removed by a small random movement of the illuminating beam. This movement causes a continuous change in fringe order of the interference fringes and washes them out to some extent. The fringes produced at the image conversion device are apparently unique to the microchannel plate type image intensifier. A single stage proximity focus type converter was tried and did not generate the troublesome pattern, but produced an unacceptably dim image.

3.5 Conclusions

Images have been produced of individual dislocations in fairly thick (111) slices of silicon. The distribution of such defects in the crystal can be observed in real time with only modest preparation of the surfaces. Apparently, all the dislocations in the slice can be seen except the pure screw segments. This technique may thus have some usefulness in the area of semiconductor device manufacturing and quality control.

4. Process Related Silicon Studies

4.1 Ribbon Silicon

Silicon crystals grown by this technique are considered to be viable candidates for photovoltaic devices. In general, the efficiency of solar cells made by this technique show lower photovoltaic efficiency than comparable cells made from Czochralski grown crystals. Their lower efficiencies are associated with defects induced during crystal growth. In an examination of ribbon grown crystals provided by G. Schwuttke of IBM, we found very large birefringent signal. The signal originated from bands running roughly parallel to the growth direction. The sign of the stress in these bands follows a sinusoidal pattern. The amplitude of the signal was suggestive of very large strains. In addition, a large density of defects could be observed. However, the density was too large for us to resolve using our current optics. In Fig. 16 we show birefringent bands, and in Fig. 17 we provide evidence for the presence of defects.

4.2 Ion Implantation Damage

Implantation was carried out on silicon single crystal wafers grown by the Czochralski technique. We attempted to observe the strain field near the boundary separating an ion-implanted region from an un-implanted area. No birefringent signal was detected. At the present time we do not know if this is a consequence of a low signal to noise ratio or that the

strain was not present. X-ray topographs of a smaple rendered amorphous by implantation also showed no strain contrast. An amorphous sample which was subsequently crystallized by a laser beam also shows little detectable birefringent signal. We believe that such signals are present but were not detected in our set-up.

4.3 Processed Devices

The birefringent technique is relatively unique in that it can provide information about small localized strains. Similar information can be obtained with x-ray topographs and by transmission electron microscopy. The limitation of the x-ray topograph is its very low or no magnification, and that of the transmission electron microscope is sample preparation, which is usually destructive.

In device fabrication, which involves high temperature processing, differential thermal expansion can lead to large stresses, which are particularly problematic at edges or corners. We examined several kinds of device structures and have obtained results which suggest that the widespread use of this technique to study such local strains will be limited by diffraction effects arising from edges. In Fig. 18 we show a series of micrographs obtained from a silicon device in which the edges produce a diffraction contrast which behaves identically to that expected from birefrining imaging. The disappearance of signal at an angle of 45° to the polarization vector is expected both from birefringent and diffraction theory. This unfortunate circumstance limits the use of the birefringent technique to study local strains associated with edges or corners.

There are a number of ways of avoiding the diffraction effect, but they all tend to limit the utility of the technique. For example, the thickness of the scattering edge material could be varied until a diffraction minima is present. The underlying strain could then be detected. Alternatively, the refractive index of the edge could be matched with a fluid. This would eliminate the diffraction effect and bring out the strain signal.

5. Summary and Conclusions

We have shown that dislocations and strain fields, in general, can be detected in GaP, garnets and silicon using birefringent techniques and state of the art detectors for 1.1μ infrared radiation. We believe that the utility of the infrared birefringent technique to studying completed Si devices on a chip are limited by diffraction effects and by the presence of metallurgy which is opaque to infrared radiation.

Our conclusion is that the birefringent technique can be developed as a very useful quality control technique in the early stages of device fabrication - such as crystal growth, slicing, and oxidation (or nitriding). Its use as the device nears completion is limited.

References

1. S. M. Hu, Appl. Phys. Letters 22 (1973) 261.
2. B. E. Argyle and P. Chaudhari, AIP Conf. Proc. 10 (1973) 403.
3. P. Petroff and R. T. Hatrman, Appl. Phys. Letters 23 (1973) 469.
4. B. Monemar and G. R. Woolhouse, Appl. Phys. Letters 29 (1976) 605.
5. W. L. Bond and J. Andrus, Phys. Rev. 101 (1956) 1211.
6. A. R. Lang, J. Appl. Phys. 30 (1959) 1748.
7. R. Bullough, Phys. Rev. 110 (1958) 620.
8. V. L. Indenbom, V. I. Nikitenko and L. S. Milevskii, Soviet Phys. Solid State 4 (1962) 162.
9. J. W. Matthews, E. Klokholm and T. S. Plaskett, IBM J. Res. Develop. 17 (1973) 426.
10. J. F. Nye, Physical Properties of Crystals (Clarendon, Oxford, 1960) p. 243.
11. C. D. West and A. S. Makas, J. Chem. Phys. 16 (1948) 427.
12. K. G. Bansiger and K. S. Iyengar, Proc. Phys. Soc. (London) 71 (1958) 225.
13. A. Rahman and K. S. Iyengar, Acta Cryst. 20 (1966) 144.
14. J. P. Szczesniak, D. Guddeback and J. C. Corelli, J. Appl. Phys. 47 (1976) 5357.
15. B. H. Kear and P. L. Pratt, Acta Met. 6 (1958) 457.
16. J. W. Matthews, T. S. Plaskett and J. Ahn, Phil. Mag. 33 (1976) 73.
17. R. W. Dixon, J. Appl. Phys. 38 (1967) 5149.
18. S. E. Blum, R. J. Chicotka and B. K. Bischoff, J. Electrochem. Soc. 115 (1968) 324.
19. S. J. Bass and P. E. Oliver, J. Crystal Growth 3 (1968) 286.
20. B. K. Tanner and D. J. Fathers, Phil. Mag. 29 (1974) 1081.
21. D. A. Jenkins and J. J. Hren, Phil. Mag. 33 (1976) 173.
22. F. C. Frank and J. F. Nicholas, Phil. Mag. 44 (1953) 1213.
23. D. A. Jenkins, Ph.D. Dissertation, University of Florida, Gainesville (1973).
24. J. W. Matthews, E. Klokholm, V. Sadagopan, T. S. Plaskett and E. Mendel, Acta Met. 21 (1973) 203.
25. B. Cockayne and J. M. Roslington, J. Mater. Sci. 8 (1973) 601.
26. J. W. Matthews, E. Klokholm, T. S. Plaskett and V. Sadagopan, Phys. Status Solidi(a) 19 (1973) 671.
27. D. J. Fathers and B. K. Tanner, Phil. Mag. 28 (1973) 749.
28. V. L. Indenbom, V. I. Nikitenko and L. S. Milevskii, Soviet Phys.-Dokl 6 (1962) 1034.
29. F. Lihl, J. Tomiser, P. Skalicky and M. Küster, Z. Angew, Physik 32 (1971/2) 287.
30. J. W. Matthews and T. S. Plaskett, Phys. Status Solidi(a) 38 (1976) 577.
31. A. H. Bobeck and E. Della Torre, Magnetic Bubbles, North Holland Publishing Co., Amsterdam, 1975, p. 114.
32. T. S. Plaskett, E. Klokholm, D. C. Cronemeyer, P. C. Yin and S. E. Blum, Appl. Phys. Lett., 25, 357 (1974).
33. C. D. Brandle and A. J. Valentino, J. Cryst. Growth, 12, 3 (1972).
34. D. C. Miller, J. Electrochem So., 120, 678 (1973).
35. W. T. Stacey, J. A. Pistorius, and M. M. Jansen, J. Cryst. Growth, 22, 37 (1974).
36. J. W. Matthews, E. Klokhom and T. S. Plaskett, AIP Conf. Proc., 10, 271 (1973).
37. M. J. Prescott and J. Basterfield, J. Mater. Sci., 2, 583 (1967).
38. K. Lal and S. Mader, J. Cryst. Growth, 22, 37 (1974).
39. J. W. Matthews, T. S. Plaskett, and J. Ahn Phil. Mag., 33, 73 (1976).
40. C. Malgrange, J. F. Petroff, M. Savage, and A. Zarka, Phil. Mag., 33, 743 (1976).
41. R. Bullough, Phys. Rev., 110, 620 (1958).
42. V. L. Indenbom and G. E. Tomilovskii, Soviet Phys., Crystallogr., 2, 183 (1957).
43. H. L. Glass, Mat. Res. Bull., 8, 43 (1973).
44. J. W. Matthews and T. S. Plaskett, phys. stat. sol. (a), 38, 577 (1976).
45. J. W. Matthews and T. S. Plaskett, phys. stat. sol. (a), 37, 499 (1976).
46. D. A. Jenkins and J. J. Hren, Phil. Mag. 33, 173 (1976).

47. J. Rabier, H. Gaiem and P. Veyssière, J. Appl. Phys., 47, 4755 (1976).
48. J. R. Patel, J. Appl. Phys., 44, 3903 (1973).
49. J. R. Patel and A. Authier, J. Appl. Phys., 46, 118 (1975).
50. J. M. Hedges and J. W. Mitchell, Phil. Mag., 44, 223 (1953).
51. J. J. Oberly, J. of Metals, 6, 1205 (1954).
52. K. Okada, J. Phys. Soc. Japan, 10, 1018 (1955).
53. V. L. Indendom, V. I. Nikitenki and L. S. Milevskii, Soviet Phys. Dokl., 6, 1034 (1962).
54. F. Lihl, J. Tomiser, P. Skalicky and M. Küster, A. angew Phys., 32, 287 (1971).

Captions to Figures

Fig. 1 Optical micrograph of dislocations in a gallium phosphide crystal one cm in thickness. The microscope was focussed on a plane 4 mm from the upper surface of the sample. Polarizer and analyzer were inclined at 45° to the borders of the figure.

Fig. 2 Micrographs of the same area of a GaP crystal. The specimen was raised 0.1 mm between (a) and (b). The displacement of the sharply imaged portions of the dislocations that accompanied this adjustment shows that the dislocations were inclided at ~34° to the imaging light beam.

Fig. 3 Micrographs at different focal settings of dislocations in a (111) wafer of NdGG. The edges of the white triangle in (a) are parallel to the <110> directions in the wafer plane. Polarizer and analyser are inclined at 45° to the borders of the figure.

Fig. 4 Micrographs at different focal settings of an (001) wafer of NdGG. (a) shows the lower surface of the wafer and (f) the upper. The edges of the etch pits are parallel to <100> directions in the wafer plane. Polarizer an analyser were inclined at 45° to the border of the figure.

Fig. 5. A pair of prismatic loops around an iridium inclusion in a (111) wafer. P is a precipitate particle formed along the dislocation line. Polarizer and analyser were inclined at 45° to the borders of the figure.

Fig. 6 A pair of dislocation loops, $L_{1,2}$ in a (100) wafer of NdGG. The portions of L_1 that are imaged in sharp focus, and the inclination of L_1 to the wafer plane, show that it was parallel to {110}. Polarizer and analyser were inclined at 45° to the border of the figure.

Fig. 7 A pair of small prismatic loops, A and B, in a (111) wafer. The <110> directions in (111) are given by the edges of the white triangle. The two micrographs are of the same specimen area. Loop A is imaged in sharp focus in (a) and B is in sharp focus in (b). Polarizer and analyser were inclined at 45° to the borders of the Figure.

Fig. 8 Micrographs of the surface and interior of an (001) wafer. The image contrast of the four dislocations near the center of the figure is consistent with their having Burgers vectors whose edge components in the wafer plane are parallel to (100). Polarizer and analyser were at 45° to the borders of the figure.

Fig. 9 A low-angle grain boundary in an (001) wafer of NdGG. The dislocations are arranged in a parallel uniformly spaced array near A but are less regularly arranged elsewhere. Polarizer and analyser were inclined at 45° to the borders of the figure.

Fig. 10 A portion of a low-angle boundary in an (001) wafer of NdGG. Polarizer and analyser were at 45° to the borders of the figure. The rotation across the boundary was about 10^{-6} degrees. The length of the scale marker is approximately equal to the resolution limit of the eye.

Fig. 11 Experimental set up.

Fig. 12 Mixed dislocations in (111) silicon wafer imaged in plane polariscope. The polarizer direction is vertical. The small dark triangles are etch pits on the specimen surface.

Fig. 13 Array of curved dislocation lines, imaged with the polarizer direction vertical and at 45° to the vertical. Notice that nearly all the dislocation contrast vanishes when the lines are in the same general direction as the polarizer/analyzer. Also note that several of the etch pits in the field have no visible dislocation line attached.

Fig. 14 Array of fairly straight dislocation lines imaged under conditions of maximum and minimum contrast (lines 45° to polarizer, lines parallel to polarizer/analyzer.) Notice the faint horizontal bands resulting from a slightly wedge shaped specimen.

Fig. 15 Small group of dislocations which pass through the specimen. The microscope is focussed about midway through the thickness, and etch pits on upper and lower

surface are visible. Notice that the etch pits on the surface are inverted relative to those on the other.

Fig. 16 Alternate light and dark bands in a silicon ribbon crystal. Curved set of parallel lines are thickness figures.

Fig. 17 Higher magnification micrograph of a light band showing breakup of bands into finer lines. Individual defects could not be resolved.

Fig. 18 Series of micrographs taken on a silicon device. Fig. (a) Straight transmission - polarizer and analyzer not crossed completely. (b) Contrast from edges when polarizer and analyzer are crossed and edge is parallel to analyzer. (c) Edge contrast disappears by rotating sample by 45°. Bright spots are from corners, which are now parallel to analyzer. In (b) these corners were out of contrast.

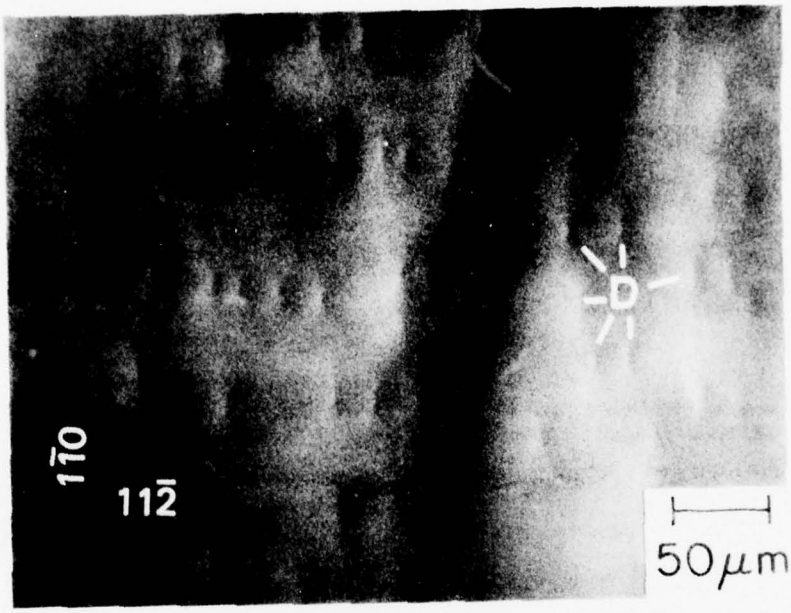

Figure 1

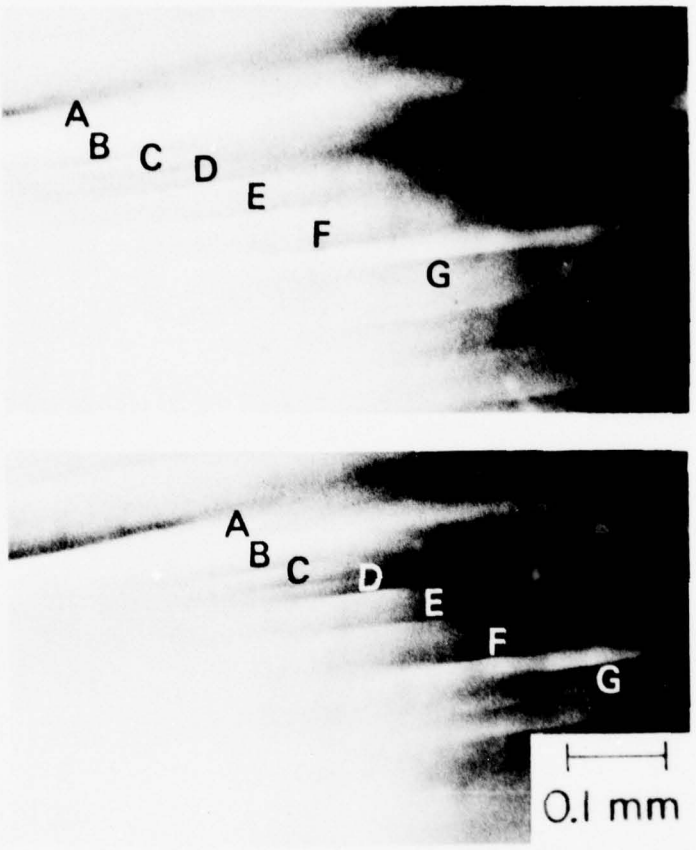

Figure 2

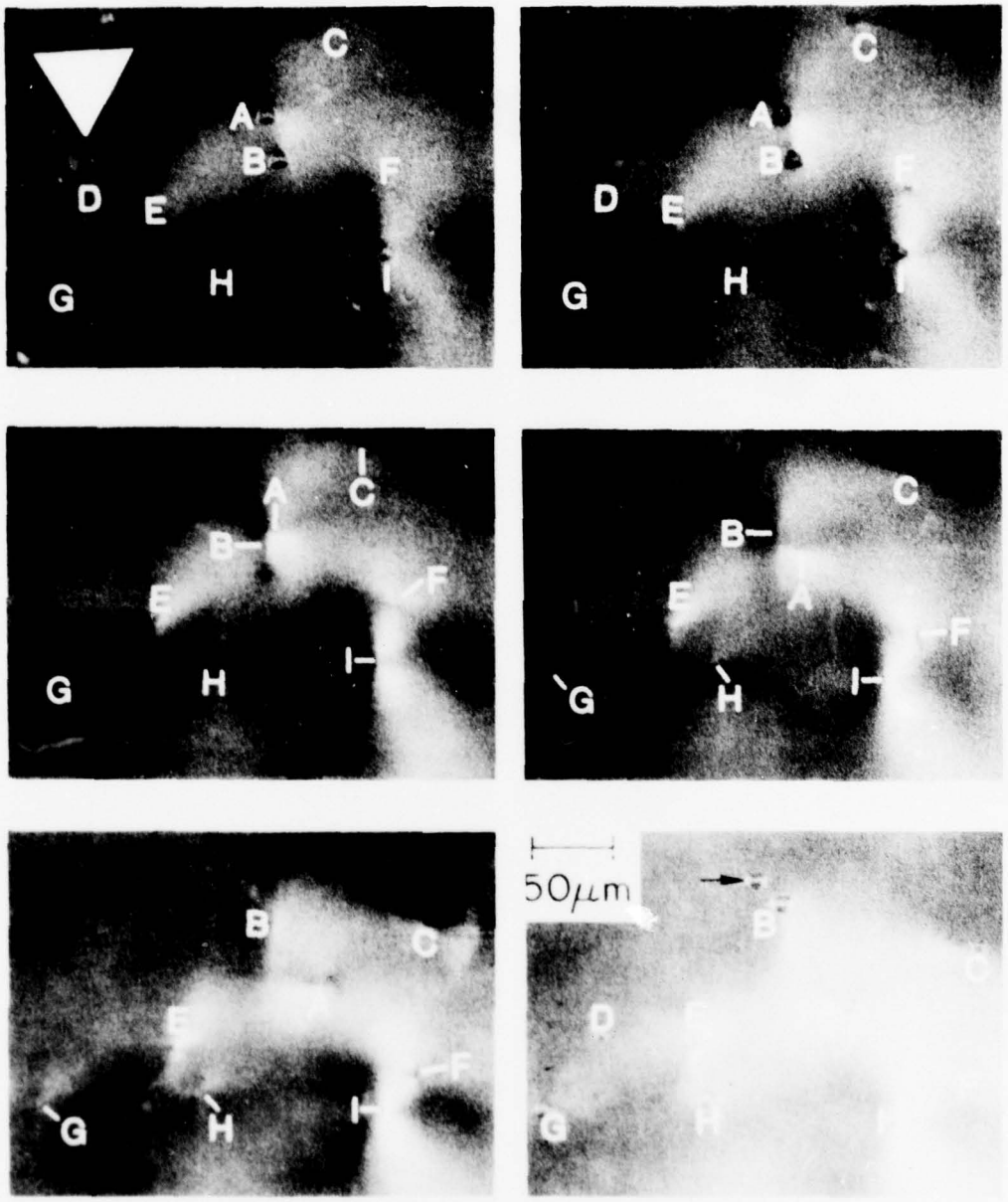

Figure 3

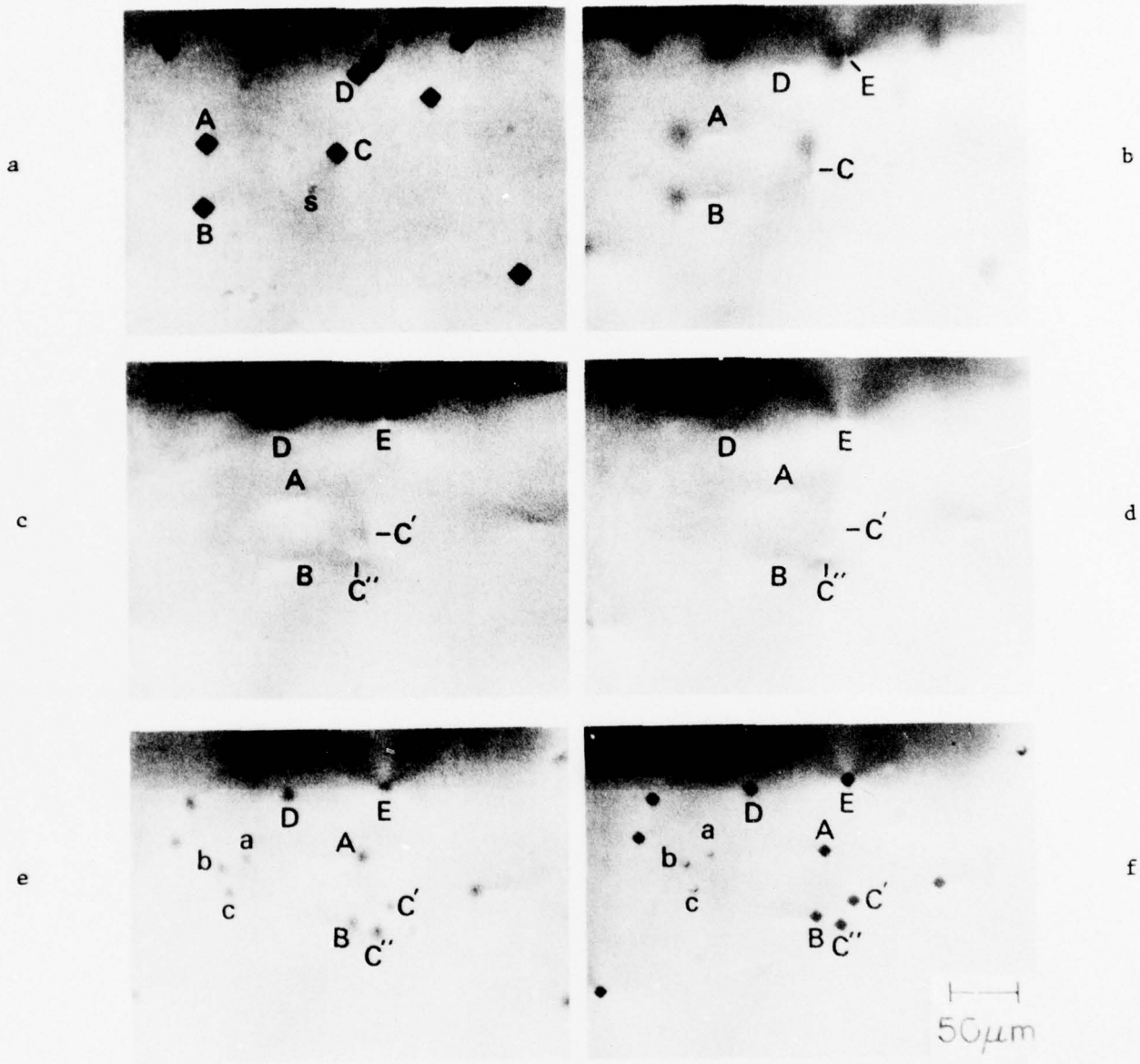
a
D
A
C
S
B
b
D
E
A
-C
B
c
D
E
A
-C′
B
C″
d
D
E
A
-C′
B
C″
e
D
E
a
b
A
c
C′
B
C″
f
D
E
a
b
A
c
C′
B
C″
50μm

Figure 4

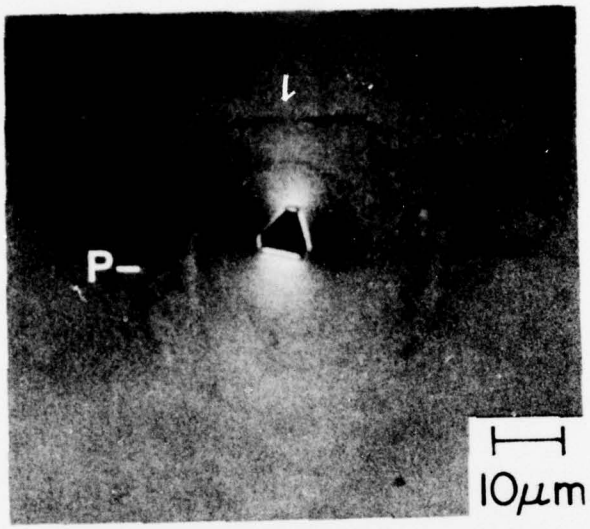

Figure 5

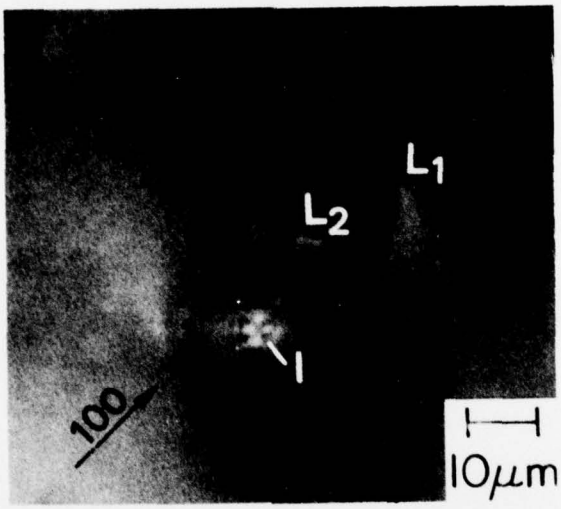

Figure 6

a

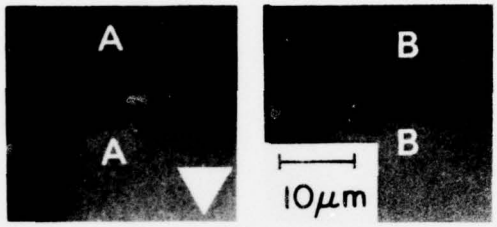

b

Figure 7

a

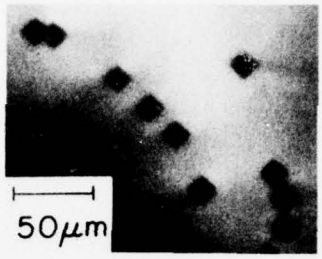

b

Figure 8

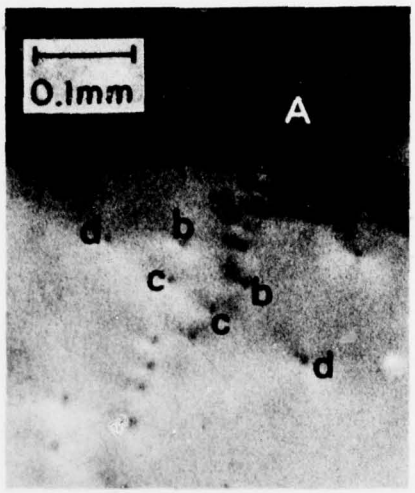

Figure 9

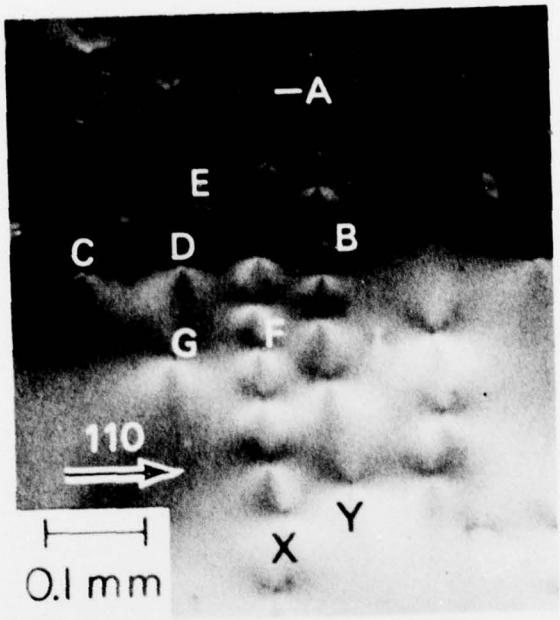

Figure 10

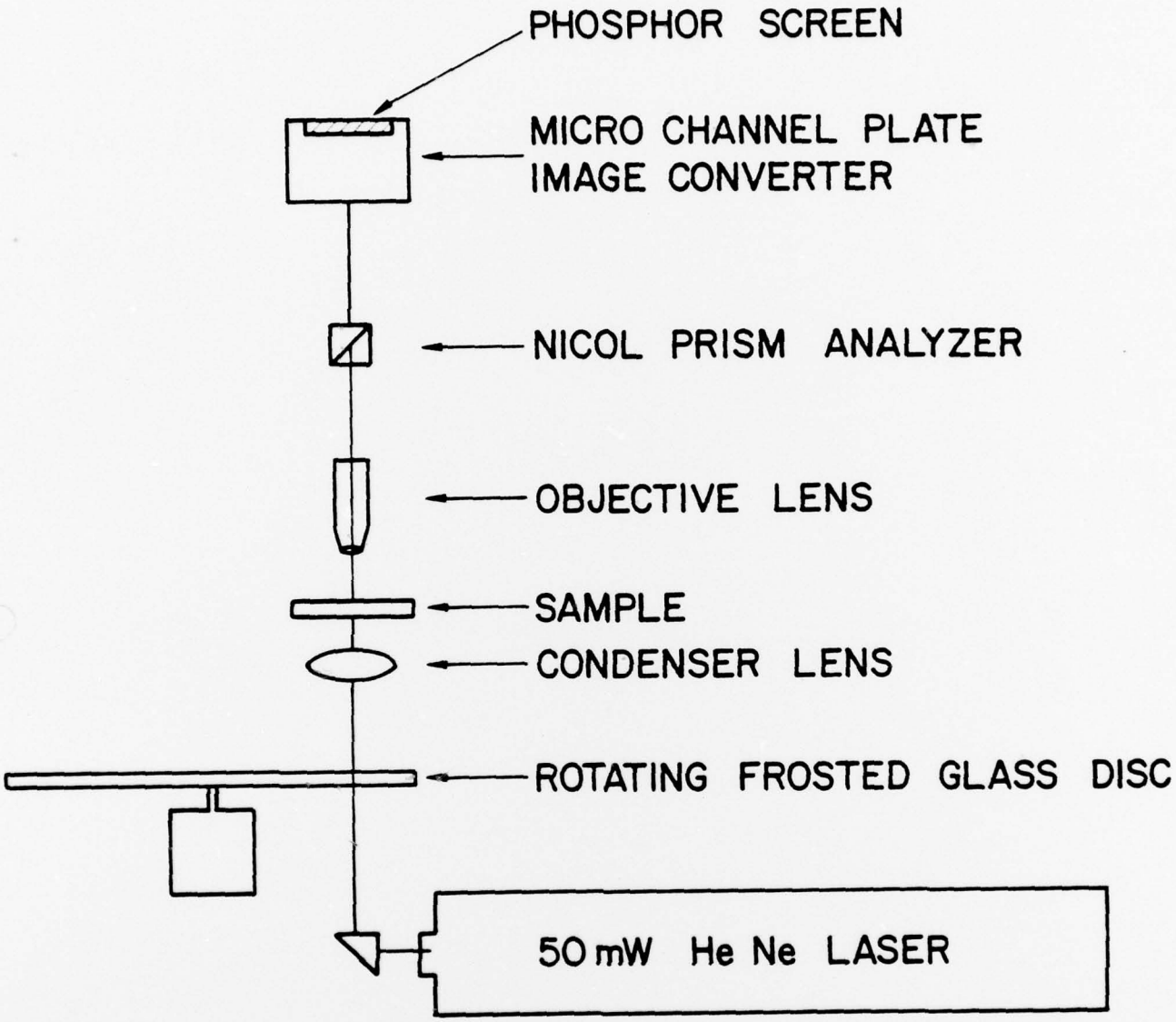

Jenkins, Plaskett, Chaudhari

Figure 11

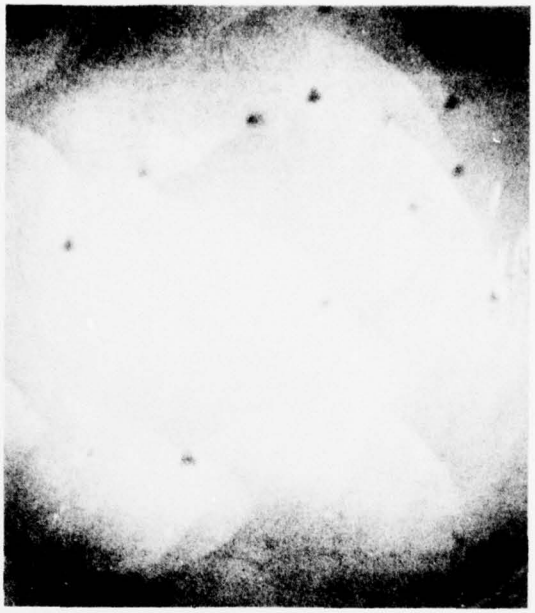

Figure 12

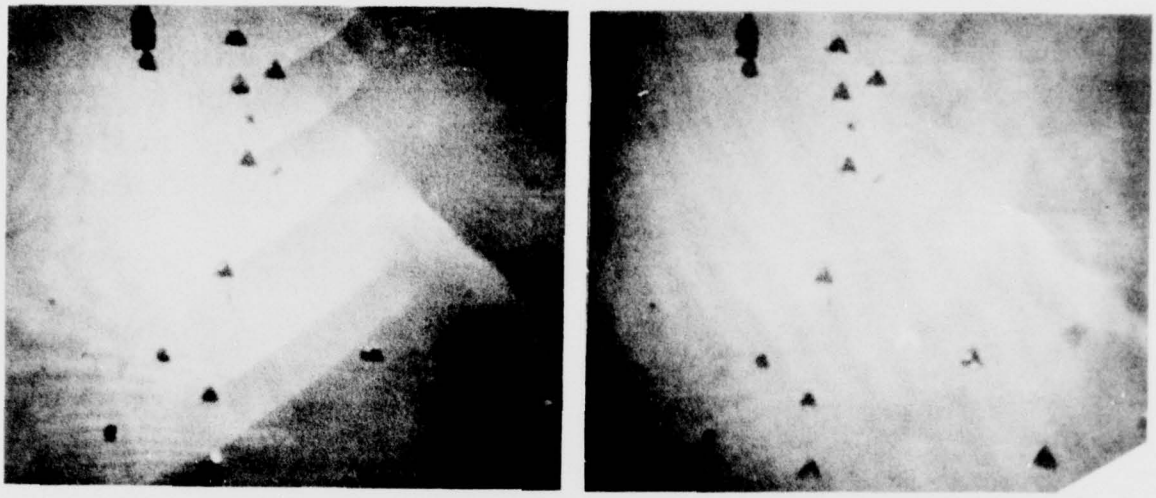

Figure 13

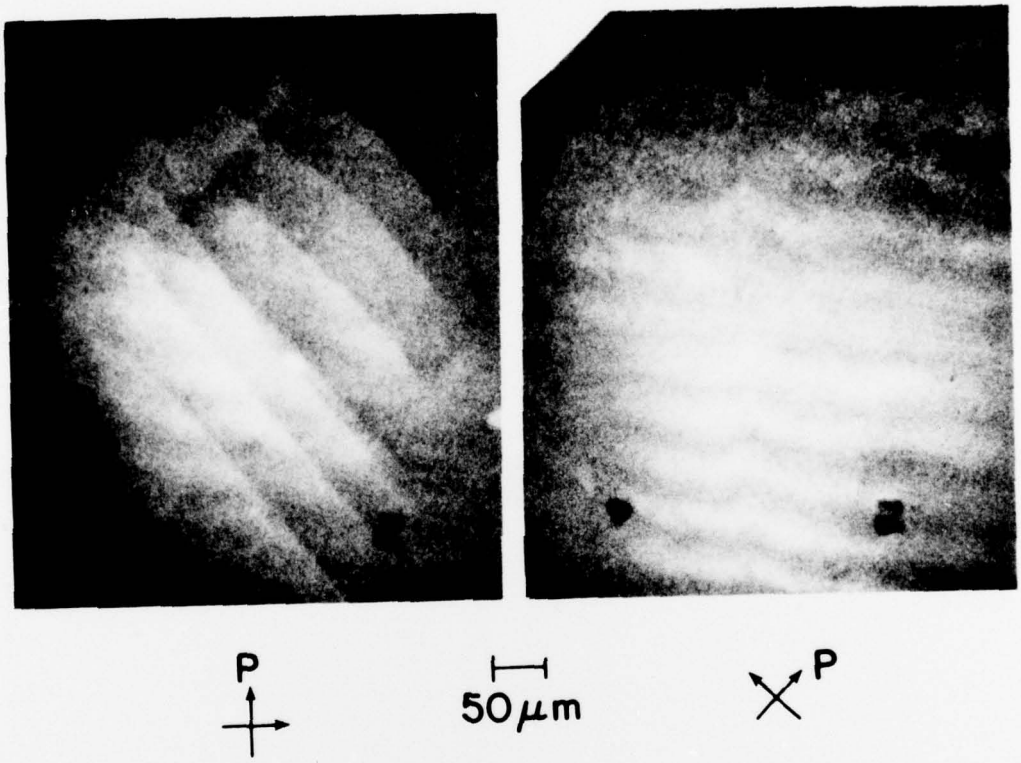

Figure 14

Figure 15

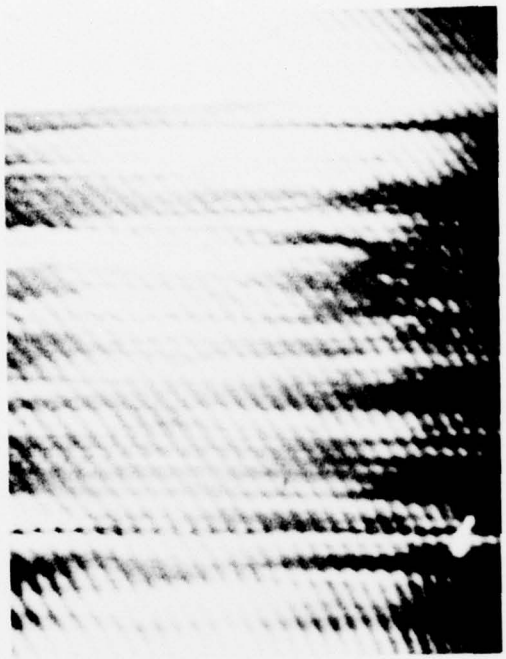

Figure 16

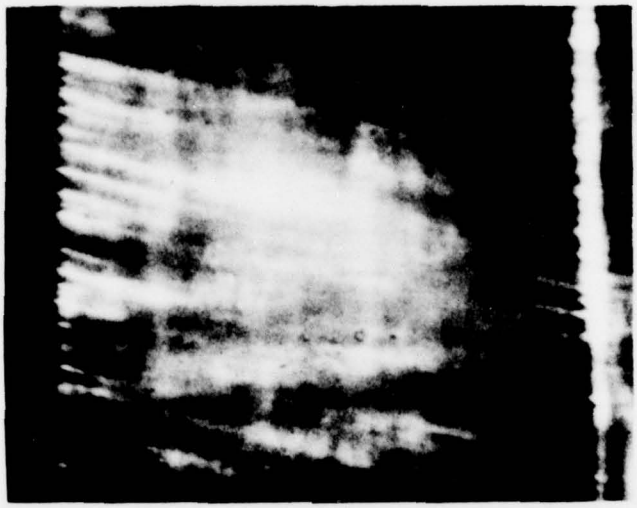

Figure 17

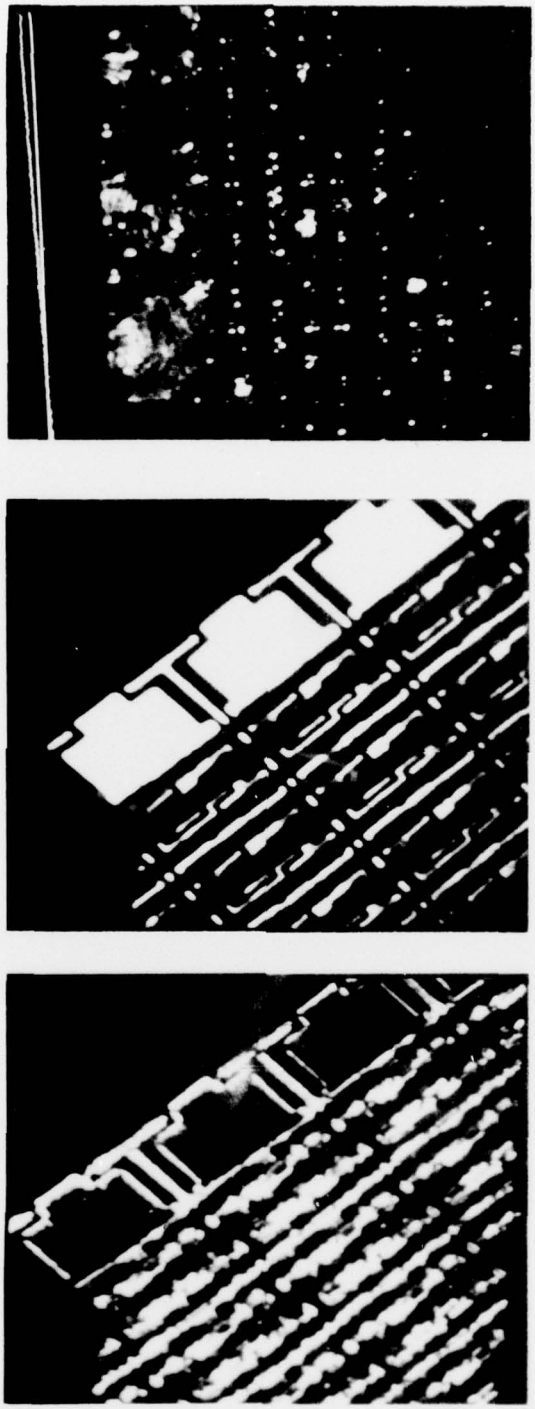

Figure 18